

We are IntechOpen, the world's leading publisher of Open Access books Built by scientists, for scientists

6,900

Open access books available

186,000

International authors and editors

200M

Downloads

Our authors are among the

154

Countries delivered to

TOP 1%

most cited scientists

12.2%

Contributors from top 500 universities



WEB OF SCIENCE™

Selection of our books indexed in the Book Citation Index
in Web of Science™ Core Collection (BKCI)

Interested in publishing with us?
Contact book.department@intechopen.com

Numbers displayed above are based on latest data collected.
For more information visit www.intechopen.com



Optoelectronic Key Elements for Polymeric Fiber Transmission Systems

Ulrich H.P. Fischer-Hirchert and Mladen Joncic

Abstract

In short-range communication 1 mm PMMA SI-POF established itself as a reasonable alternative to the traditional data communication media such as glass fibers, copper cables, and wireless systems. Due to multiple advantages such as a large core diameter, tolerance to fiber facet damages, and low installation costs, the SI-POF is already applied in industrial automation, automotive industry, and in-house/office networks. To experimentally demonstrate the feasibility and potential of a high-speed POF WDM concept, a four-channel data transmission setup was realized. A four-legged multiplexing POF bundle was developed to combine the signals from four visible laser diodes onto SI-POF link. For the separation of wavelength channels, the interference filter-based demultiplexer with two-stage configuration was used. It was shown that POF WDM with lower channel rates and simple transmission technique (NRZ + FFE) could provide aggregate bit rates comparable to those achieved with the single-wavelength systems that used advanced modulation formats (DMT or PAM + DFE) and required significant signal processing. In addition, the 50 m SI-POF link at an aggregate bit rate of 7.8 Gb/s was demonstrated over 50 m SI-POF, respectively, at the BER = 10^{-3} .

Keywords: polymeric fiber transmission, WDM over POF, optical DMT modulation, optical PAM modulation

1. Introduction

Having its origin in the 1960s as well as the silica glass fiber, the polymer optical fiber (POF) stayed long in the shadow of the huge development and success of glass fiber communications. However, the advances in POF technology and the growing need for high-speed short-range communication networks make POF nowadays gain more and more importance. The key advantage of POF is a large core diameter. It makes POF tolerant to the fiber facet damages and relaxes the alignment tolerances, thus also reducing the installation costs. Furthermore, POF is pliable, durable, and inexpensive; offers small weight and short bend radius; allows easy installation, simple termination, and quick troubleshooting; and also provides the immunity to electromagnetic interference. Due to its diverse advantages, in short-range applications POF established itself as a reasonable alternative to the traditional data communication media such as glass fibers, copper cables, and wireless systems (see **Table 1**).

Transmission medium	Data rate	Distance	Safety	Cost	Handling	Installation	Total
Twisted pair cable	+	0	0	++	—	0	2+
Coaxial cable	0	0	0	+	0	0	1+
Glass fiber	++	++	++	—	—	—	1+
Polymer fiber	0	—	++	+	+	+	4+
Wireless	—	—	—	++	++	++	1+
Powerline	—	—	—	+	+	++	0

Table 1.

Comparison of different transmission media. Characteristics between very bad (--) and particularly good (++) [1].

Today, POF is produced with different core materials, core diameters, and index profiles. A comprehensive overview on various POFs is given in [1]. Two major POF types are made of polymethyl methacrylate (PMMA) and perfluorinated (PF) materials. The parameters of the common PMMA and PF POFs are specified in the IEC Standard 60793-2-40, which defines eight different POF classes [2]. The PMMA POF is produced with both step-index (SI) and graded-index (GI) profile, whereas the PF POF offers only GI profile. The GI profile of the core ensures high modal bandwidth exceeding $1.5 \text{ GHz} \times 100 \text{ m}$ for the PMMA POF and $300 \text{ MHz} \times 1 \text{ km}$ for the PF POF. However, the implementation of the PMMA GI-POF is confined to 500–680 nm wavelength range due to the high optical attenuation at other wavelengths ($>400 \text{ dB/km}$). In contrast, the PMMA SI-POF suffers from intermodal dispersion limiting the bandwidth-length product to around $50 \text{ MHz} \times 100 \text{ m}$ but also provides several attenuation windows in the visible spectrum (400–700 nm). Due to its advantages over the other POF types such as technological maturity, ease and cost of production, and high numerical aperture (NA), the standard 1 mm PMMA SI-POF (POF class A4a.2 according to IEC 60793-2-40) is the best known and by far the most widely employed type of POF. This is also the fiber this work concentrates on.

In vehicles SI-POF displaces copper in the network structure of a passenger cabin for multimedia data services. The infotainment communication system known as Media Oriented System Transport (MOST) connects different multimedia components in the SI-POF-based ring topology [3], as illustrated in **Figure 1**. The current (third) version of the MOST system (MOST150) supports the data transfer at 150 Mb/s over link lengths of about 10 m.

Another sector where SI-POF displaces traditional communication media are short-range networks in houses and offices. As an in-house extension of a broadband access network (e.g., VDSL, HFC, FTTB), the typical application of POF technology is the delivery of triple-play services (combination of broadcasting, telecommunication, and the Internet) to the end user. The Fast Ethernet transceivers (100 Mb/s) and since 2013 also the Gigabit Ethernet transceivers (1 Gb/s) are available on the market enabling the transmission of broadband services over 50 m SI-POF. The Gigabit solutions from KD-POF employing the multilevel signaling and from Teleconnect based on the multicarrier modulation are accompanied by the technical standards ETSI TS 105175-1-2 [4] and ITU-T G.9960, Annex F [5], respectively.

The commercial communication systems with SI-POF use a single channel for data transmission. However, the transmission performances of SI-POF are impaired by strong intermodal dispersion and high optical attenuation. Stimulated by the growing bandwidth demands (e.g., 10–40–100 Gb/s Ethernet speed), various concepts to overcome the low-pass characteristic of SI-POF have been successfully demonstrated over the last few years. The simplest solutions utilized passive

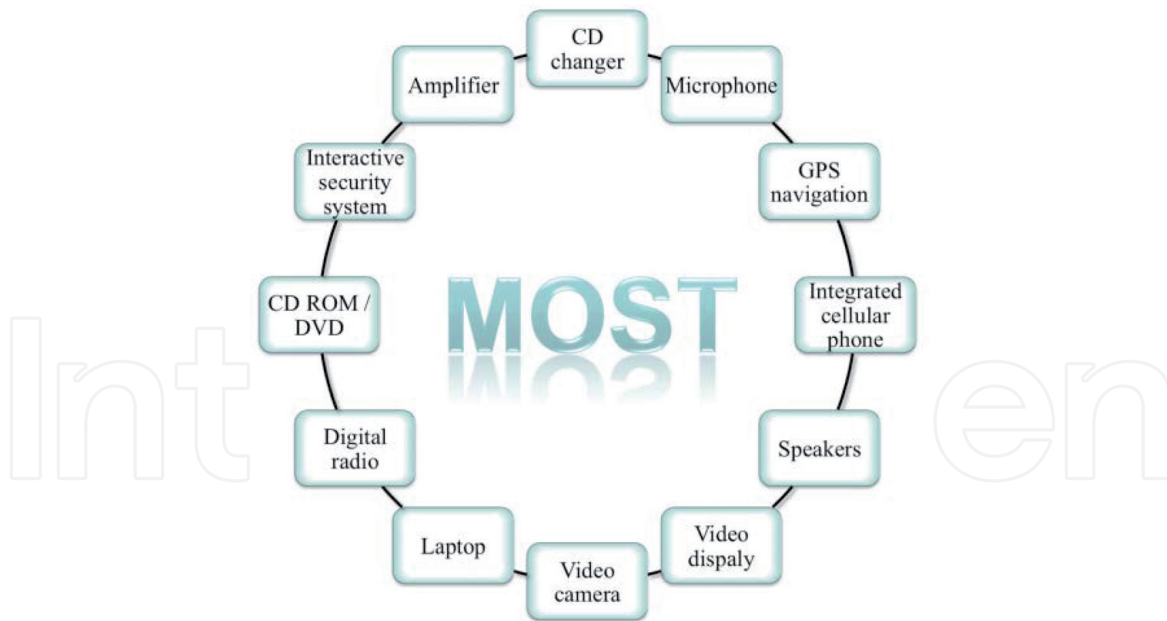


Figure 1.
 SI-POF-based ring topology of a MOST system in a car.

equalization implemented as an analog high-pass filter that increased the electrical -3 dB bandwidth of a channel [6]. A major focus was also placed on the digital signal processing techniques, which were mostly implemented offline due to the lack of commercial components. Both the non-return-to-zero (NRZ) and the spectrally efficient multilevel signaling were combined with the digital receiver equalization to increase the data rates over SI-POF [7, 8]. The sophisticated spectrally efficient multicarrier modulation formats were also successfully implemented to combat the highly dispersive SI-POF channel [9, 10].

Complying with any of the hitherto developments, utilization of several optical carriers for parallel transmission of data channels over a single fiber represents another alternative to increase the transmission capacity of SI-POF. The technique is well-known as wavelength division multiplexing (WDM). The principle of WDM is shown in **Figure 2**. Since different wavelengths λ_1 – λ_N do not interfere with each other in a linear medium, they can be used to simultaneously carry the data signals over a single fiber. Thereby, the capacity of a fiber, i.e., of an optical communication system, increases almost proportionally with the number of wavelength channels.

Two components are essential for WDM, a wavelength multiplexer and demultiplexer. The multiplexer combines the signals at different wavelengths, coming from different transmitters, onto a single fiber. On the opposite side of the optical link, the demultiplexer performs an inverse function, separating the wavelength channels to be detected by separate receivers.

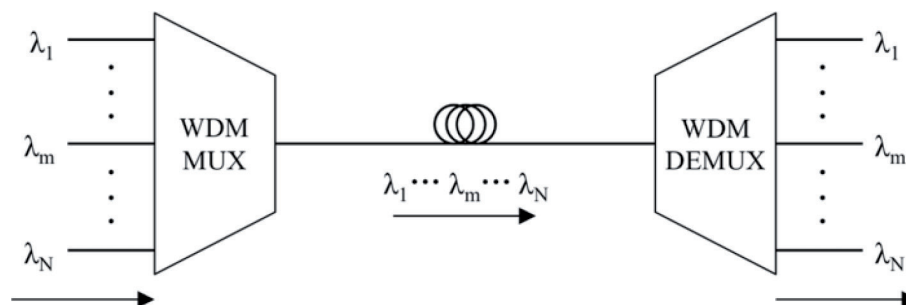


Figure 2.
 Principle of WDM: MUX, multiplexer; DEMUX, demultiplexer.

The existing WDM components developed for single-mode glass fibers in the infrared region, such as Mach-Zehnder interferometers, arrayed waveguide gratings or fiber Bragg gratings, cannot be reused for a highly multimode SI-POF. On the other hand, the operating principles of demultiplexers based on thin-film interference filters and on a diffraction grating can be applied for POF. In spite of some other demultiplexing solutions (e.g., employing dispersion prisms), these two demultiplexing techniques have been recognized as the most promising for SI-POF. However, because of the difference in the operating wavelength range, fiber diameter, NA, etc., compared to the glass fibers, such demultiplexers must be newly designed for SI-POF communication. An overview of the state-of-the-art thin-film interference filter-SI-POF demultiplexers will be given. The first aim of this work is to further investigate experimentally these demultiplexing techniques for SI-POF. Accordingly, the aim of this work is to demonstrate experimentally high-speed POF WDM data transmission offering capacity increase compared to the single-channel systems.

2. Fundamentals of WDM for short-range communication over POF

2.1 Transmission properties of 1 mm PMMA SI-POF

The 1 mm PMMA SI-POF is the best known and by far the most widely employed type of POF. It is made of 980 μm diameter PMMA core surrounded by a thin cladding (10 μm) made of fluorinated polymer. The typical spectral attenuation of SI-POF is shown in **Figure 3**. The fiber supports operation in the visible spectrum from 400 to 700 nm. The lower wavelength bound is determined by the degradation of the PMMA compound with prolonged exposure to the ultraviolet (UV) wavelengths shown in [11] and in [12]. The attenuation value of around 400–450 dB/km, which still allows operation over shorter link lengths (<20 m), sets the upper wavelength bound.

Two intrinsic loss mechanisms contribute to the raise of attenuation at shorter and particularly UV wavelengths. The electronic transitions due to the absorption of light in the polymer compound cause absorption peaks in the UV region. However, their absorption tails extend through the visible spectrum affecting the POF attenuation [13]. The dependence of the attenuation coefficient of electronic transitions α_e [dB/km] on the wavelength for PMMA is given by [14]:

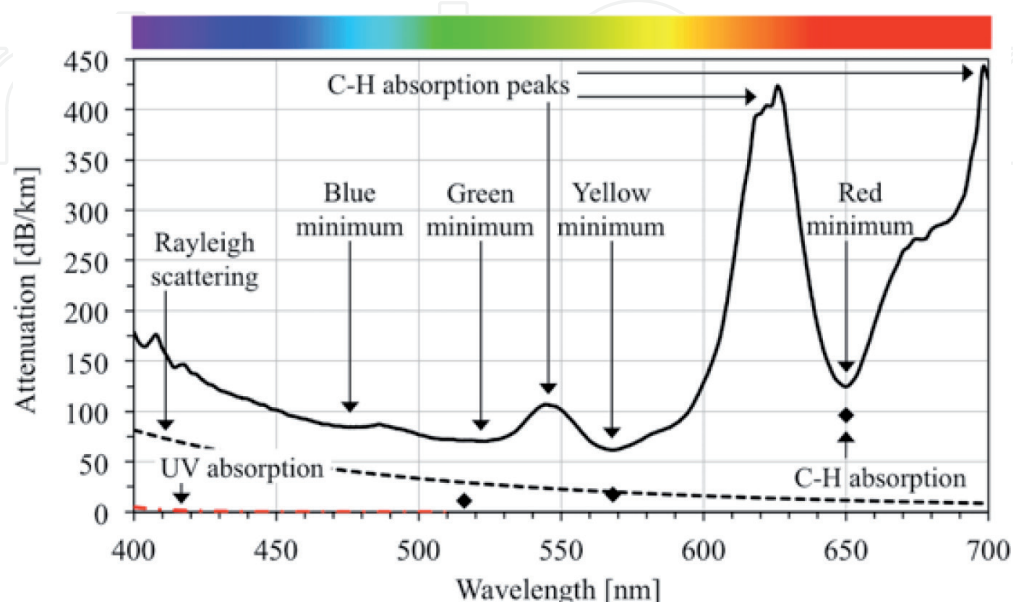


Figure 3. Typical spectral attenuation of 1 mm PMMA SI-POF [13] with contributions of intrinsic loss mechanisms and with attenuation minima and maxima.

$$\alpha_e = 1.58 \cdot 10^{-12} \exp\left(\frac{1.15 \cdot 10^4}{\lambda}\right). \quad (1)$$

The second loss mechanism is the Rayleigh scattering. It is caused by the structural irregularities in the polymer compound that are much smaller than the wavelength of light (order of one tenth of wavelength or less). The effect of scattering becomes more pronounced as the wavelength decreases since the scattering attenuation coefficient α_s [dB/km] is inversely proportional to the fourth power of the wavelength shown by Kaino [15]:

$$\alpha_s = 13 \cdot \left(\frac{633}{\lambda}\right)^4 \quad (2)$$

In the infrared region, the attenuation significantly increases due to the intrinsic absorption losses caused by vibrations of the molecular C-H bonds (total of eight per MMA monomer). The higher overtones of the C-H bond vibrations also extend in the visible spectrum. The seventh overtone at 549 nm and particularly the sixth and the fifth overtone at 627 and 736 nm, respectively, cause pronounced absorption peaks and wide absorption bands, predominantly determining the level of attenuation in the red spectral range shown by Emslie [16] and by Groh [17].

The contributions of the intrinsic loss mechanisms to the overall attenuation of SI-POF are also shown in **Figure 3**. The wavelength regions where the fiber exhibits low attenuation are called attenuation windows. The SI-POF has four attenuation windows. Those are blue, green, yellow, and red windows, with the absolute attenuation minimum of approx. 62 dB/km at around 568 nm (yellow window). The parameters of the attenuation windows are listed in **Table 2**.

The mean refractive index of SI-POF core material in the visible spectrum is $n_{core}=1.492$, whereas the refractive index of cladding is $n_{clad}=1.412$. Due to the big difference in refractive indices of core and cladding, the numerical aperture (NA)

$$NA = \sqrt{n_{core}^2 - n_{clad}^2} \quad (3)$$

has the value of 0.482 (usually rounded to 0.5). The corresponding maximum acceptance angle of the fiber is 30°. The large core radius $a_{core} = 490 \mu\text{m}$ combined with the high NA results in the normalized frequency v

$$V = 2\pi \frac{a_{core}}{\lambda} \cdot NA \quad (4)$$

of 2698 at 550 nm, which is far above the limit $v = 2.405$ below which a fiber is in single-mode operation. The number of modes N_{mod} propagating through SI-POF can be approximated as

$$N_{mod} \approx V^2/2, \quad (5)$$

Attenuation window	Blue	Green	Yellow	Red
Attenuation minimum [dB/km]	85	70	62	125
Wavelength of the attenuation minimum [nm]	476	522	568	650
Approximate 3 dB width of the window [nm]	19	24	8	4

Table 2.
 Attenuation windows of SI-POF (based on the attenuation curve from **Figure 2**).

corresponding to 3.64 million modes at 550 nm. Due to the significant path difference between lower- and higher-order modes, propagating respectively at smaller and larger angles relative to the optical axis, the strong intermodal dispersion is inherent to SI-POF. In the time domain, it is manifested as pulse broadening, thus introducing the inter-symbol interference (ISI). In the frequency domain, the intermodal dispersion results in a low-pass frequency response, constraining the bandwidth-length product of SI-POF to around 50 MHz \times 100 m shown by Ziemann et al. [18].

3. Demultiplexing employing thin-film interference filters

The technology based on thin-film interference filters is mature and one of the most commonly applied technologies for realization of WDM demultiplexers in single-mode glass fiber communication. The demultiplexers for coarse WDM applications cascade the interference filters to provide up to 16 flattop channels between 1271 and 1611 nm, with 20 nm minimum channel spacing [19]. The typical parameters of commercial 4-, 8-, and 16-channel demultiplexers with IL <1.6, 2.7, and 3.7 dB, respectively, can be found in [20]. The thin-film filter-based demultiplexers for dense WDM applications are commercially available with up to 40 channels in 1550 nm region and <8 dB IL. Instead of simply cascading the filters, those devices usually employ a modular configuration described in by Dutta et al. [21]. The same reference provides a typical transfer function of the 40-channel demultiplexer with 3–6 dB IL and 100 GHz (0.8 nm) channel spacing.

In the visible spectrum, and thus within the application range of SI-POF, a vast variety of thin-film interference filters is available from various manufacturers. Even though not particularly intended for POF applications, the visible interference filters represent an attractive solution for POF demultiplexers, where wavelength selectivity, low IL, and high isolation are required.

A dichroic mirror is a special type of interference filter intended for the spatial separation or combination of light at different wavelengths. It is designed to operate at 45° AOI, such that a certain spectral range is transmitted, whereas the rejected wavelength range is reflected at 90° angle with respect to the incident optical axis. A commercial visible spectrum dichroic mirror has a transition slope between the transmission and reflection band of typically 30–40 nm (see **Figures 3** and **4**). This is significantly less steep compared to the standard interference filters designed for

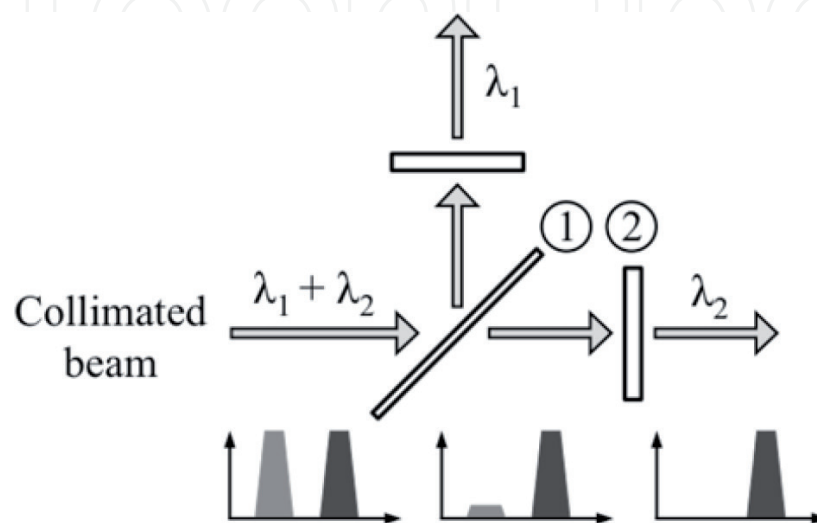


Figure 4. Principle of separation of two collimated wavelength channels employing thin-film interference filters: (1) dichroic mirror (45° AOI); (2) interference filter (0° AOI).

the normal incidence. Unlike an interference filter, e.g., a long-pass mirror must be not only highly transmissive above the cutoff wavelength but also highly reflective below it. Therefore, producing steeper slopes would require increased complexity of the coating and, accordingly, a significant rise in production costs.

The interference filters show significant angular dependence of their transmission characteristic measured by Lee et al. [22]. To be applicable for SI-POF, the highly divergent beam from the fiber must be transformed into a bundle of parallel rays prior to the incidence. To increase the channel isolation, an additional band-pass filtering in each of the output channels should be implemented prior to the focusing of light. As an example, a selection of the dichroic mirror and interference filters for demultiplexing two wavelength channels centered around $\lambda_1 = 450$ nm and $\lambda_2 = 525$ nm is shown in **Figure 4**.

3.1 Data transmission techniques for increasing the channel capacity

Two data transmission techniques were used to overcome the bandwidth limitation of a POF WDM channel, which is primarily caused by the intermodal dispersion of SI-POF. Those were:

1. Non-return-to-zero (NRZ) modulation in combination with electronic dispersion compensation, in particular feed-forward equalization (FFE)
2. Discrete multitone (DMT) modulation

In the single-channel POF systems with intensity modulation and direct detection (IM/DD), those are well-known techniques for increasing the channel capacity. The next two subsections briefly introduce the two techniques: non-return-to-zero modulation and feed-forward equalization.

According to the Nyquist theorem for two-level signaling, the maximum bit rate (in bits per second) for a noiseless channel of the bandwidth B equals $2B$. Since the real systems encounter noise, this theoretical limit cannot be achieved. Therefore, for 100 m SI-POF link, the data rates less than 100 Mb/s are possible. If the data rate further increases, the eye diagram of the received signal becomes partially or completely closed due to the combination of the ISI and additive noise (introduced, e.g., by receiver's transimpedance amplifier).

The equalization techniques are used to open the eye diagram at the receiver for clock and data recovery (CDR). In its principle, the equalizer compensates for ISI, which is deterministic (unlike the random noise) and determined by the low-pass frequency response of a POF channel. In the work a simple linear FFE equalization technique was employed to correct the distorted signal waveforms at the receiver.

An FFE equalizer is realized as a discrete-time finite impulse response filter with adjustable coefficients. The output of the equalizer is obtained as the weighted sum of the delayed samples of the input signal as

$$V_e(t) = \sum_{k=0}^{N-1} c_k V_r(t - k T_D), \quad (6)$$

where $V_e(t)$ is the equalized voltage sample at the time t , c_k is the equalizer coefficient (weighting factor), T_D is the tap delay, and $V_r(t - k T_D)$ is the k times delayed uncorrected received voltage sample. A block diagram of the FFE equalizer is shown in **Figure 5**.

Through its coefficients the equalizer may synthesize a transfer function corresponding to the inverted channel frequency response, thus eliminating the ISI. In

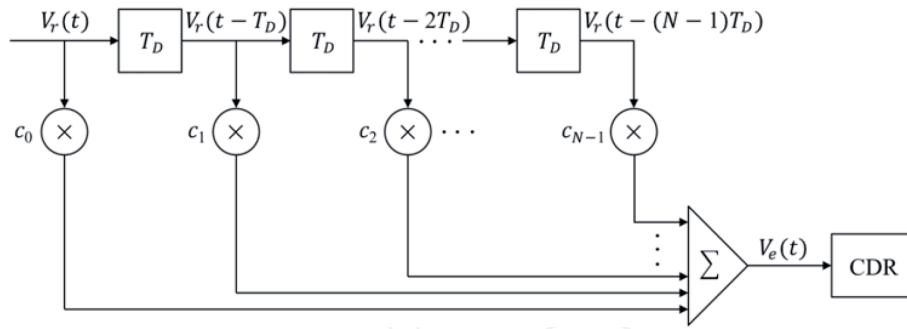


Figure 5.
Basic structure of an FFE equalizer.

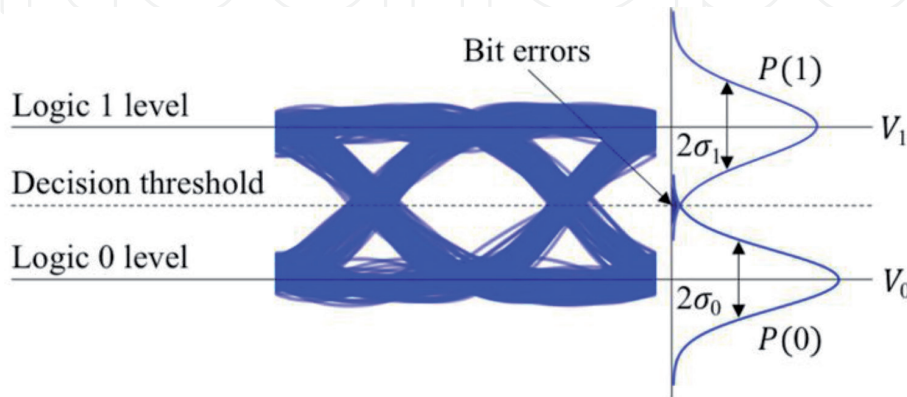


Figure 6.
Calculation of the Q -factor from the eye diagram: $P(1)$ and $P(0)$, probability distributions of received logic 1 and 0 levels, respectively.

a noisy POF channel, and due to inverting the channel frequency response, this would lead to great noise amplification at higher frequencies where the channel frequency response is small in magnitude. Typically, to minimize the probability of the decision error, the weighting factors are calculated to minimize the noise power at the cost of a certain amount of residual ISI after equalization. The descriptions of different algorithms for optimizing the equalizer coefficients can be found in Loquai et al. [23].

The BER performance of the system was estimated based on the Q -factor of the equalized eye diagram (**Figure 6**)

$$Q = \frac{V_1 - V_0}{\sigma_1 - \sigma_0}, \quad (7)$$

where v_1 and v_0 are the mean values and σ_1 and σ_0 are the standard deviations of the equalized signal voltages associated with logic 1 and 0 levels, respectively, as shown in **Figure 6**. The corresponding BER was obtained as

$$BER(Q) = \frac{1}{2} \operatorname{erfc}\left(\frac{Q}{\sqrt{2}}\right), \quad (8)$$

where $\operatorname{erfc}(x) = (2/\sqrt{\pi}) \int_x^\infty \exp(-\tau^2) d\tau$ is the complementary error function.

3.2 DMT: discrete multitone modulation

To provide high spectral efficiency of the signals transmitted within POF WDM channels, a DMT modulation technique was used. The DMT is a multicarrier modulation format and represents a baseband version of a better-known

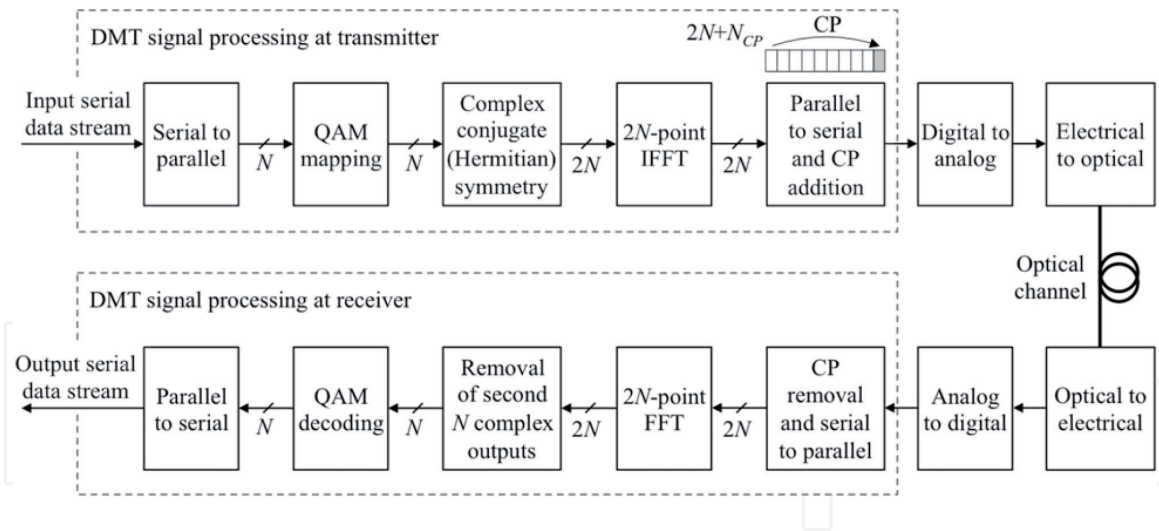


Figure 7.
 Principle of DMT transmission over an optical IM/DD channel: N CP, length of CP.

orthogonal frequency division multiplexing (OFDM). Unlike the OFDM, which is used in wireless communication systems such as wireless local area networks (WLAN), the DMT is widely employed as enabling technology for digital subscriber lines (DSL), e.g., asymmetric DSL (ADSL) and very high DSL (VDSL). The DMT-based transmission was also shown to be very beneficial for SI-POF communication by Joncic et al. [24], Diaz et al. [25], and Vinogradov et al. [10].

The DMT technique slices the frequency-selective channel into a large number of subchannels that can be considered to have a flat frequency response. Each subchannel is then used for transmission of a passband signal with quadrature amplitude modulation (QAM). The simultaneous transmission of the low-speed parallel streams reduces the influence of the ISI. Another important property of DMT is that it adapts the signal parameters (QAM size and power in each subchannel) to the characteristic of the communication channel.

The principle of the DMT transmission over an optical IM/DD channel is shown in **Figure 7**. A high-speed serial data stream is first divided into N parallel lower-speed streams, where N corresponds to the number of subcarriers. Every M bits in each stream are grouped together and mapped into a complex value corresponding to a point of the QAM constellation with 2^M size. The modulation of the complex values onto N different subcarrier frequencies is based on the inverse fast Fourier transform (IFFT). To obtain real-valued time domain signal samples at the output of the IFFT block, a $2N$ -point IFFE has to be carried out. Thereby, the second half of $2N$ IFFT inputs must be complex conjugate of the first half and symmetric around the middle of the input vector, a property referred to as a Hermitian symmetry. The real-valued samples of the DMT time signal are then parallel-to-serial converted, and a cyclic prefix (CP) is added as a guard interval at the beginning of each DMT frame to resist to inter-frame interference occurring in a band-limited channel. After digital-to-analog conversion, a bipolar continuous-time DMT frame is produced. It is then DC-biased to modulate the intensity of an electrical-to-optical converter.

At the receiver, the DMT waveform is direct-detected, analog-to-digital and serial-to-parallel converted, and demodulated using $2N$ -point fast Fourier transform (FFT). The first N complex outputs of the FFT block are QAM-decoded and parallel-to-serial converted to result in an output serial data stream.

4. POF demultiplexer employing thin-film interference filters

This chapter focuses on the experimental realization of a thin-film interference filter-based SI-POF demultiplexer using a modular and precisely adjustable setup. In a step-by-step approach, the intermediate solutions with two and three channels were first established. In addition, two different configurations of the target demultiplexer setup with four channels were realized. The principle of operation and the approach for experimental realization are explained for the simplest case of a two-channel demultiplexer. The same basic principles also apply to the demultiplexers with higher channel count.

4.1 Operating principle and measurement results for a four-channel demultiplexer

By extending the channel count to four, it was possible to investigate two different demultiplexer configurations. Those were:

- Serial configuration
- Two-stage configuration

The principle of operation of a four-channel demultiplexer with serial configuration is shown in **Figure 8**. In this configuration the dichroic mirrors were cascaded such that each mirror (except the last one) demultiplexed a single-wavelength channel while passing all other wavelengths.

For practical realization 425, 505, and 567 nm cutoff long-pass dichroic mirrors were cascaded so that the interference filters centered at 405, 450, 525, and 650 nm could be implemented in the output ports 1–4, respectively. The corresponding transfer function and the basic parameters of the demultiplexer are shown in **Figure 9** and **Table 3**, respectively. The factors contributing to high IL in the output ports 3 and 4 are discussed in the next subchapter.

The principle of operation of a four-channel demultiplexer with two-stage configuration is shown in **Figure 10**. The first stage of the demultiplexer, represented by a dichroic mirror that follows directly after the collimating lens, splits the

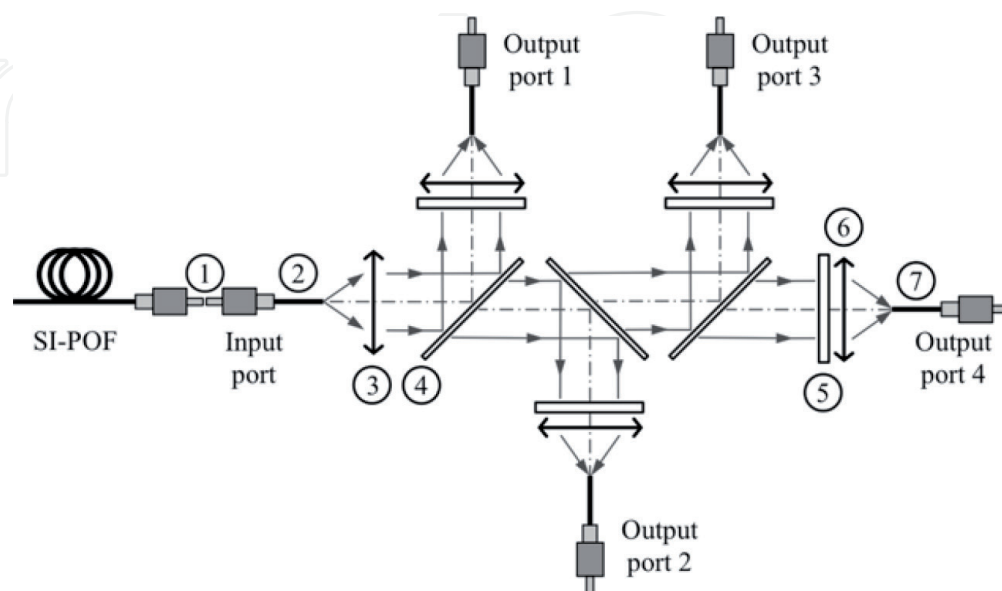


Figure 8. Principle of operation of a four-channel SI-POF demultiplexer with serial configuration (see enumeration in **Figure 3**).

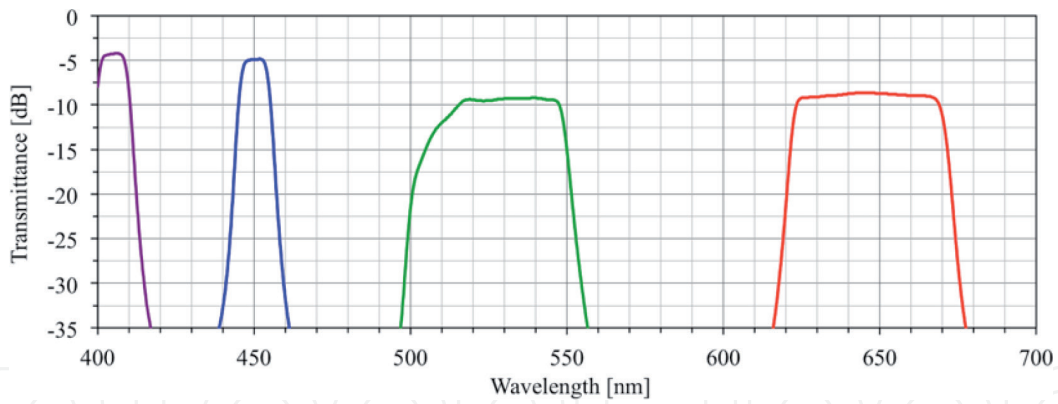


Figure 9. Transfer function of the four-channel demultiplexer with serial configuration and the channels centered at 404.9, 450.1, 529.1, and 646.4 nm.

Output port	1	2	3	4
Center wavelength [nm]	404.9	450.1	529.1	646.4
3 dB passband bandwidth [nm]	9.4	9.2	39.6	47.8
Minimum IL [dB]	4.24	4.86	9.21	8.63
IL uniformity [dB]	4.97			
(Non)adjacent channel isolation [dB]	>30			

Table 3. Basic parameters of the four-channel demultiplexer with serial configuration.

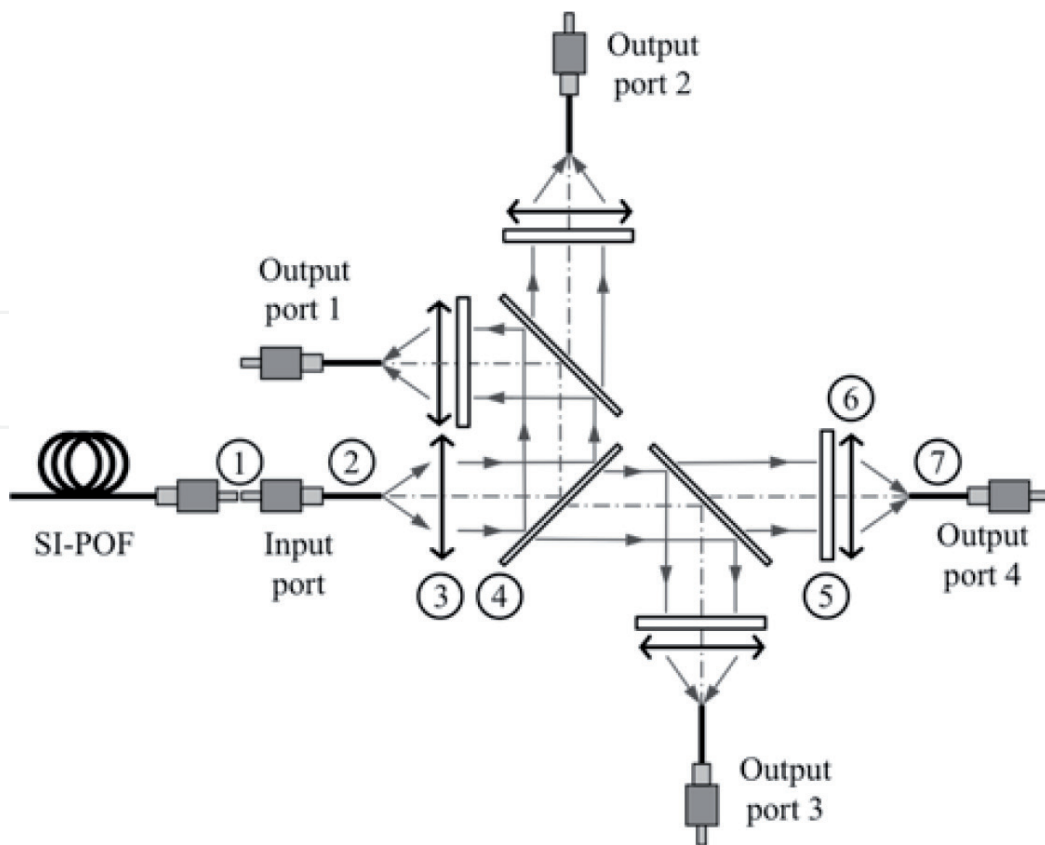


Figure 10. Principle of operation of a four-channel SI-POF demultiplexer with two-stage configuration (see enumeration in Figure 8).

incident spectrum into two spectral bands. The separation of the individual wavelength channels was then performed within the second stage of the demultiplexer. The corresponding laboratory setup is shown in **Figure 11**.

The practical realization was carried out with 505 nm cutoff long-pass dichroic mirror in the first stage of the demultiplexer. It reflected the lower spectral band so that 425 nm cutoff dichroic mirror was used in the second stage to demultiplex the signals for the output ports 1 and 2 in which 405 and 450 nm filters were employed, respectively. The upper spectral band transmitted by 505 nm mirror was demultiplexed in the second stage by 567 nm dichroic mirror. The filters centered at 525 and 650 nm were used in the output ports 3 and 4, respectively.

The corresponding transfer function is shown in **Figure 12**. The basic parameters of the demultiplexer are given in **Table 4**. The measurement results for the four-channel demultiplexer with two-stage configuration were presented at the International Conference on Plastic Optical Fibers (ICPOF) 2013 [26]. To comply with all other measurements shown in this chapter, which were performed 2 years thereafter, the demultiplexer setup was assembled and characterized

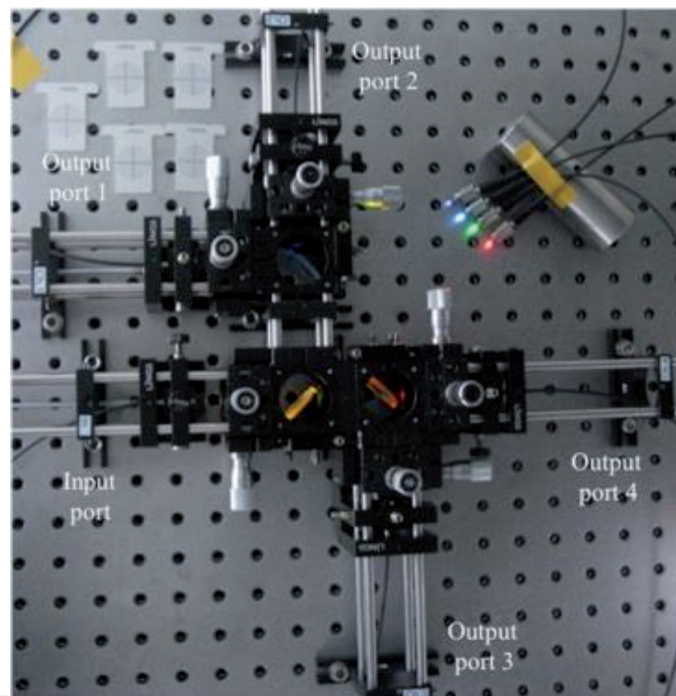


Figure 11.
Laboratory setup of the four-channel demultiplexer with two-stage configuration.

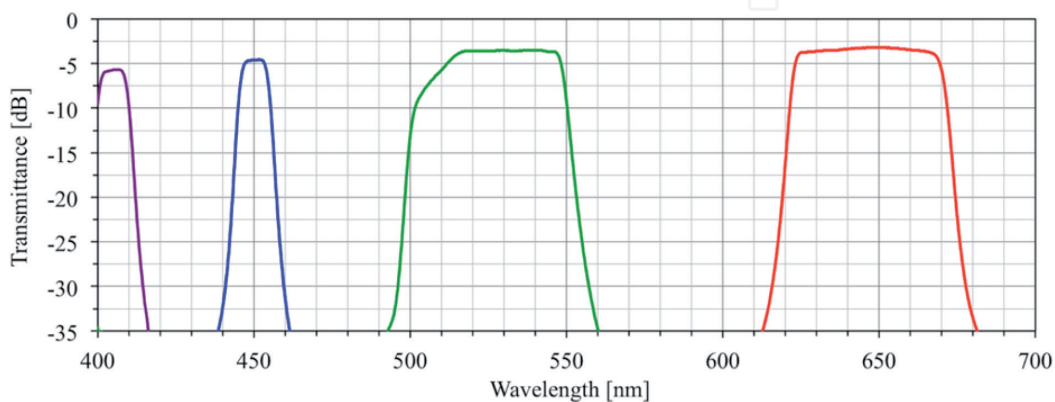


Figure 12.
Transfer function of the four-channel demultiplexer with two-stage configuration and the channels centered at 404.9, 450.1, 528.3, and 646.4 nm [26].

Output port	1	2	3	4
Center wavelength [nm]	404.9	450.1	528.3	646.4
3 dB passband bandwidth [nm]	9.4	9.3	41.6	47.6
Minimum IL [dB]	5.66	4.55	3.47	3.19
IL uniformity [dB]			2.47	
(Non)adjacent channel isolation [dB]			>30	

Table 4.
Basic parameters of the four-channel demultiplexer with two-stage configuration [26].

again. While preserving the same principal behavior of the spectral response, the minimum IL in the output ports 1 to 4 was 6.15, 5.44, 4.21, and 3.85 dB, respectively. Those were by 0.49, 0.89, 0.74, and 0.66 dB higher values than those reported by Appelt et al. [26].

5. Discussion

The transfer functions shown in **Figures 9** and **12** comprised for each demultiplexer channel:

- Loss of the connector interface at the demultiplexer input
- Attenuation of 1 m ingoing and 1 m outgoing SI-POF
- Propagation losses through the setup between the fiber end faces

The loss of the connector interface was minimized by applying the index-matching gel. This loss downscaled the transfer function of the demultiplexer by approx. 0.5 dB. To obtain the performance of the optomechanical setup itself, the value of 0.5 dB should be added to the measured transmittance values. The propagation losses included the Fresnel loss at the end face of the ingoing and the outgoing fiber, the losses introduced by the optical components (including reflections on the anti-reflection coatings), and the coupling losses due to the setup misalignments, optical aberrations, and clear aperture of components. For the perfectly aligned components and for given distances between them (obtained, e.g., from the CAD model), the minimum loss of the demultiplexer could be estimated by means of an optical ray tracing software. However, that work was beyond the scope of this work.

The shape of the spectral response of each demultiplexer channel was predominantly determined by an interference filter that was used. Those filters provided flat-top response, steep transition slopes, and high isolation between the channels due to an optical density greater than 4 (transmission of <0.01%) in the rejection bands within 400–700 nm region. The deviations of the channels from the nominal central wavelengths and bandwidths of interference filters comply with the center wavelength and passband bandwidth tolerances of ± 2 and ± 5 nm for 10 and 50 nm filters, respectively. An exception is the green channel where the spectral response curve was truncated by 505 nm cutoff dichroic mirror with the transmission band starting at 520 nm.

The four-channel demultiplexer introduced an additional channel in the short wavelength region. That allowed simultaneous operation at the violet and blue wavelengths, which are both very attractive for POF communication due to the availability of commercial laser diodes. Two different demultiplexer configurations offered significantly different performance.

In the serial configuration, the longer wavelength channels corresponded to the higher output ports. Because of the longer optical path than the shorter wavelength channels, the longer wavelength channels:

- Were more sensitive to alignment inaccuracies
- Encountered more optical components (dichroic mirrors)
- Suffered from stronger optical aberrations
- Experienced increased beam radius due to the beam divergence caused by the finite size of the source fiber [27]

The influence of those effects can be observed in the transfer function from **Figure 12**, where the green and red channels experienced significantly higher IL than the violet and blue ones. If the effect of alignment inaccuracy, which is a parameter related to the particular setup adjustment, would be disregarded, all other effects that are inherent to the serial configuration would lead to the same principal behavior of the transfer function.

The Appelt et al. [26] demultiplexer outperformed the four-channel solution from [28] in terms of IL and especially crosstalk. An exceptional performance of that demultiplexer with IL between 3.19 and 5.66 dB (overall minimum IL of 16.87 dB) may be explained by a very precise alignment of the components. However, all other measurements (performed 2 years thereafter) with two-, three-, and four-channel setups, which had to be each time newly aligned, showed somewhat higher IL but also very consistent behavior to one another. Therefore, it cannot be excluded that some other factors such as accumulated dust on the optical surfaces or coating damages due to improper handling could have introduced additional attenuation compared to [26] measurement, which was performed with brand new components. In spite of that, all subsequent measurement results, including the IL of 3.85–6.15 dB for the reassembled two-stage demultiplexer, can be considered as excellent achievements.

The significance of these and of the other previously realized interference filter-based SI-POF demultiplexers is that they enable realization of POF WDM systems and investigation on their data-carrying capacity. For these reasons it is important to further optimize the realized demultiplexer setup and extend the channel count.

6. WDM transmission employing NRZ modulation

This subchapter shows the initial experimental setup and gives the measurement results prior and after the first optimization step. Even though performed measurements cannot be considered as real WDM, the setup with multiplexer and demultiplexer along the optical path was assembled, and its functionality was demonstrated.

6.1 Experimental setup

The data transmission setup is shown in **Figure 13**. It comprised an Agilent N4903A bit error rate tester (BERT), four butt-coupled edge-emitting laser diodes, multiplexing POF coupler, 10 m SI-POF link, interference-based POF demultiplexer, optical receivers, and Agilent 86100B sampling oscilloscope.

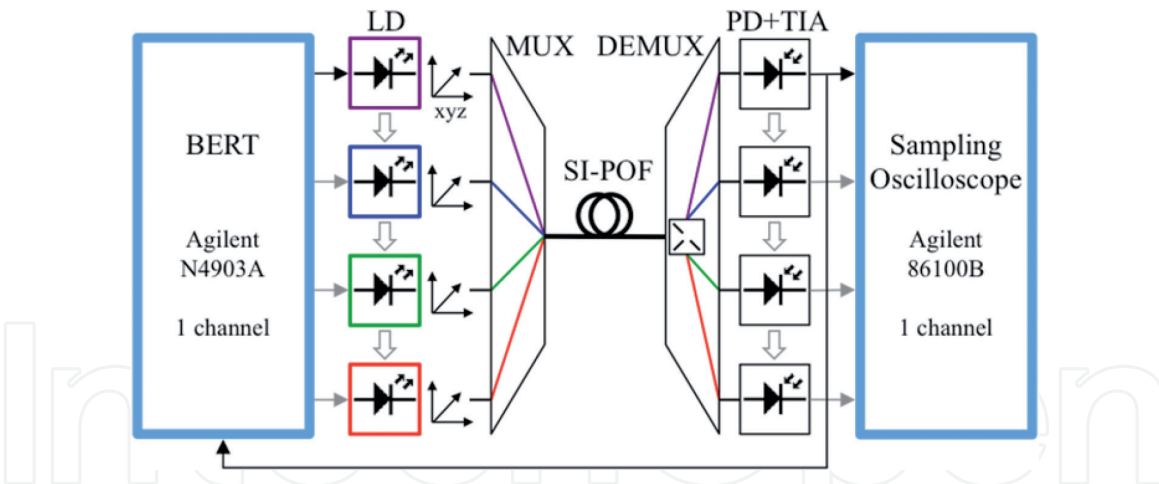


Figure 13. Experimental setup for the measurements employing NRZ modulation: LD, laser diode; MUX, multiplexer; DEMUX, demultiplexer; PD, photodiode; TIA, transimpedance amplifier.

To provide precise temperature control, prevent possible damage from overheating, and extend the lifetime, the laser diodes were mounted in Thorlabs TCLDM temperature-controlled laser diode mounts. The temperature of an integrated temperature control (TEC) element of the mount was adjusted to +15°C. Only for OSRAM samples the cooling at +10°C was used to provide better stability of the optical output power. Both the temperature of the TEC element and the bias current were controlled over a Thorlabs ITC8022 module. Four of those modules were installed in a Thorlabs PRO8000 modular chassis for the simultaneous control of four operating diodes (see **Figure 15**). To maximize the coupling efficiency from the laser diode into the fiber, a butt-coupling unit based on an xy -translator (0.25 mm pitch of the adjustment screws) was utilized. The translator was mounted on the TCLDM9 mount over a 4-rod construction system, as shown in **Figure 15**. To combine the optical signals with different wavelengths onto the SI-POF link, a Comcore 4 × 1 fused POF coupler was used (see **Table 5**).

6.2 Measurement results and discussion

6.2.1 Gb/s transmission over 10 m SI-POF

The laser diodes providing the signals at four different wavelengths operated at 405 (DL-5146-101S), 450, 515, and 660 nm. Each diode was inserted into a laser socket of the TCLDM mount, which was also equipped with an internal 500 MHz bandwidth bias tee and had separate inputs for the bias and modulating current. The respective data rates achieved in the individual WDM channels were 0.5, 0.5, 0.7, and 0.8 Gb/s. The corresponding eye diagrams are represented in **Figure 14**. The effect of pulse shaping due to the low-pass characteristic of the fiber can clearly be recognized, e.g., in 405 nm channel.

Operating wavelength [nm]	405	450	515	639
Laser diode-to-coupler port launching loss [dB]	1.5	1.3	1.3	1.5
IL of 4 × 1 fused POF coupler [dB]	7.9	8.9	8.1	8.6
Connector loss (with index-matching gel) [dB]	0.5			
Total loss [dB]	9.9	10.7	9.9	10.6

Table 5. Optical power loss at the transmitter side when using 4 × 1 fused POF coupler.

The irregular signal trajectories, e.g., in the eye diagrams of 515 and 660 nm channels, indicate the presence of nonlinearities in the electrical domain (presumably introduced by the bias tee circuit). No BER measurement data were saved. However, due to the eye diagrams still opened wide enough, it can be reasonably assumed that the corresponding BERs were below the FEC threshold of 10^{-3} , allowing for the error correction.

High optical isolation of the demultiplexer provided very low optical crosstalk between the WDM channels. The crosstalk of ≤ 35 dB, coming from 450 nm channel, was detected in 515 nm channel. In all other channels, the crosstalk lower than -45 dB was detected with a Melles Griot 13 PDH 005 integrating sphere. Considering the amplitude levels of the recorded eye diagrams and low interchannel crosstalk, no reduction in the SNR of the received signals could be assumed if the laser diodes were modulated simultaneously. Therefore, it can be stated that an aggregate bit rate of 2.5 Gb/s could be transmitted over 10 m SI-POF with four

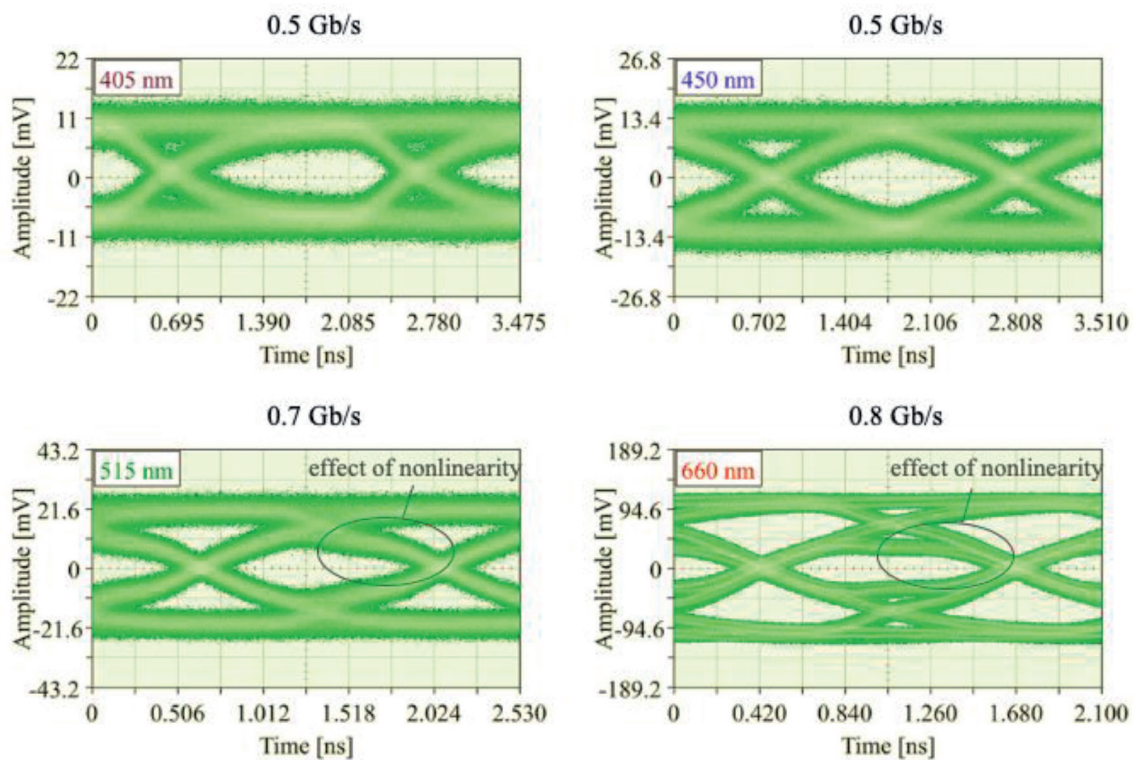


Figure 14. Eye diagrams for 10 m SI-POF link at an aggregate bit rate of 2.5 Gb/s (note: The full time scale was automatically set by the oscilloscope and is smaller than two unit intervals of the signal).

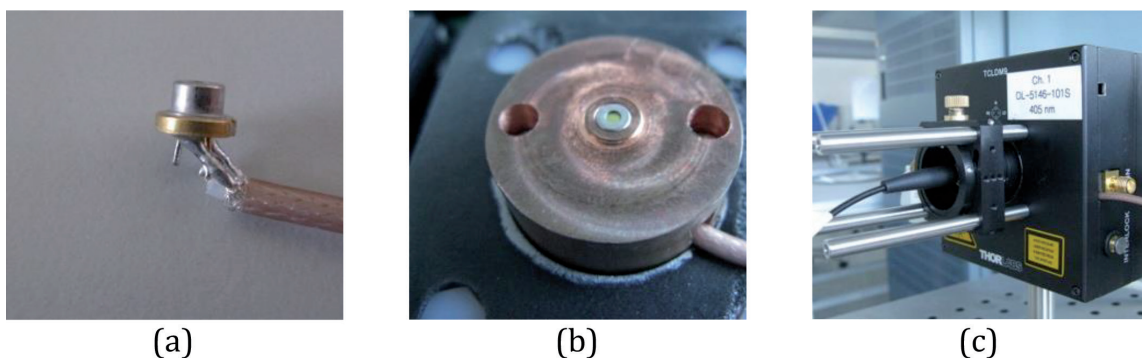


Figure 15. TO-56 diode mounted in a retainer ring; (c) TCLDM9 mount with a butt-coupling unit.

simultaneously active channels and no interchannel errors. The corresponding information rate after deduction of 7% FEC overhead would be 2.33 Gb/s.

6.3 5 Gb/s transmission over 10 m SI-POF

In the next experiment, 405 (DL-5146-101S), 450, 515, and 639 nm laser diodes were used as WDM optical sources. To directly modulate the diodes with a higher modulation bandwidth, each diode was soldered to a 50 ohm SMA formable coax cable (**Figure 14**), which was connected to the output of an external bias tee with 6 GHz bandwidth and 0.1 MHz low cutoff frequency.

Due to the low impedance of the laser diodes (typically 2–5 ohms), a severe impedance mismatch was present. However, by using higher power of the modulating signals, the mismatch could be compensated. For mounting the diodes into the mounts, copper retainer rings for both TO-56 and TO-38 packages were fabricated (**Figure 15**). For better thermal conductivity between the TEC element of the mount, the retainer ring, and the laser diode housing, a heat-conductive paste was applied on the contact surfaces.

The bit rates in the individual channels were 1.25 Gb/s (405 nm channel), 1.05 Gb/s (450 nm channel), 1.25 Gb/s (515 nm channel), and 1.45 Gb/s (639 nm channel). The transmission parameters for the individual channels are listed in **Table 6**. In contrast to the previous measurement, no signal nonlinearities were present, and the maximum achievable data rates were limited by the ISI.

Taking into account the amplitude levels of the recorded eye diagrams and low interchannel crosstalk, like in the previous experiment, no power penalty due to crosstalk could be assumed if the laser diodes were modulated simultaneously. Therefore, it can be stated that 5 Gb/s transmission could be realized over 10 m SI-POF link at the BER $<10^{-4}$ with four simultaneously active channels and no interchannel errors. Using a standard Reed-Solomon (255,247) FEC with 3.2% redundancy, 4.84 Gb/s transmission could be achieved at the BER $<10^{-9}$ [28].

6.4 WDM transmission employing NRZ modulation and FFE equalization

This subchapter shows the improved experimental setup and gives the measurement results of the simultaneous four-channel NRZ transmission over 50 m SI-POF. To mitigate the effects of ISI, the FFE equalization was implemented at the receiver side. The experimental setup is shown in **Figure 16**. It comprised a four-channel Agilent M8190A arbitrary waveform generator (AWG), four butt-coupled edge-emitting laser diodes, four-legged multiplexing POF bundle, SI-POF link of two different lengths, interference-based POF demultiplexer, Graviton SPD-2 receiver, and four-channel Agilent DSA91604A real-time oscilloscope with built-in software for digital signal processing. A photo of the general setup for investigating four-channel high-speed POF WDM transmission is shown in **Figure 17**.

To multiplex the signals from four laser diodes onto the SI-POF link, a four-legged POF bundle was used. A multiplexing interface is formed by positioning the fiber bundle against 1 mm SI-POF.

Operating wavelength [nm]	405	450	515	639
Bit rate [Gb/s]	1.25	1.05	1.25	1.45
BER	$6 \cdot 10^{-5}$	$7 \cdot 10^{-5}$	$1.1 \cdot 10^{-6}$	$9 \cdot 10^{-7}$

Table 6.
Transmission parameters for 10 m SI-POF link at an aggregate bit rate of 5 Gb/s.

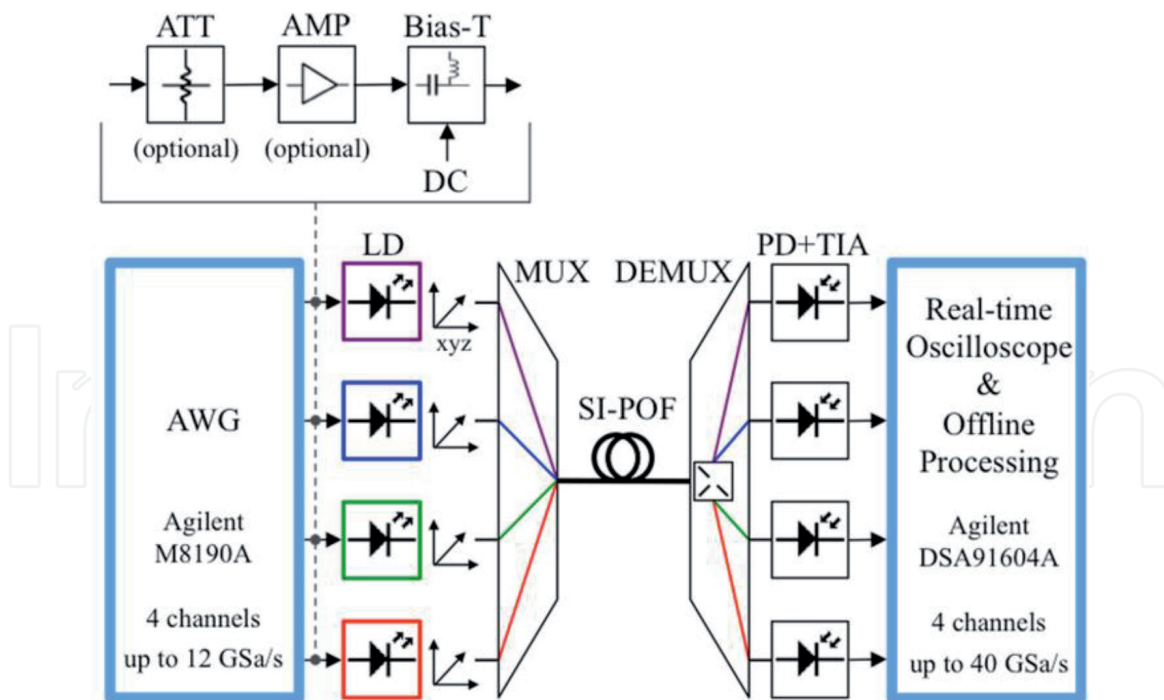


Figure 16.

Experimental setup for the measurements employing NRZ modulation and offline-processed FFE: ATT, attenuator; AMP, amplifier; DC, direct current.

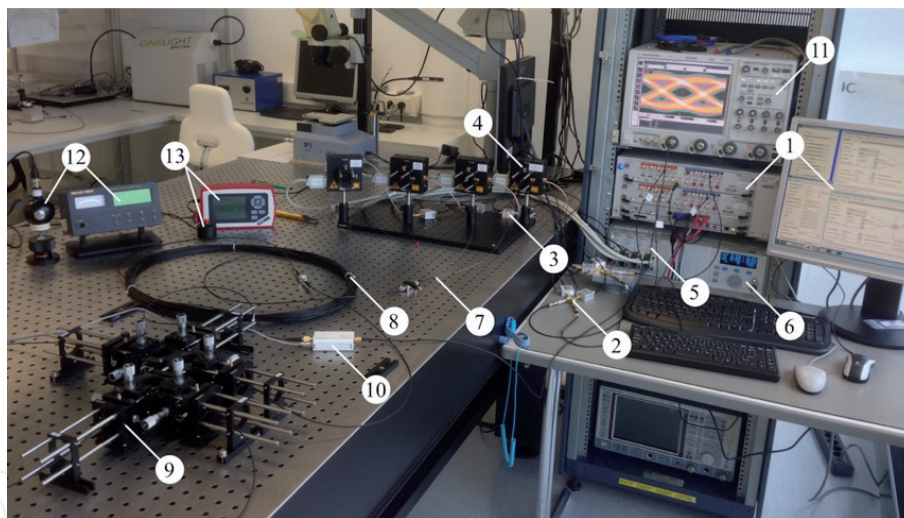


Figure 17.

Experimental setup for investigating four-channel high-speed POF WDM transmission: (1) Agilent M8190A AWG; (2) attenuator and MERA-556+ wideband amplifier; (3) bias tee; (4) Thorlabs TCLDM temperature-controlled laser diode mount; (5) Thorlabs ITC8022 module; (6) Thorlabs PRO8000 modular chassis; (7) four-legged multiplexing POF bundle; (8) SI-POF link; (9) four-channel interference filter-based demultiplexer; (10) graviton SPD-2 receiver; (11) Agilent DSA91604A real-time oscilloscope; (12) Melles Griot universal optical power meter with 13 PDH 005 integrating sphere; (13) Thorlabs PM100D power meter with S140C integrating sphere.

For realization of the bundle, an Asahi KASEI DB-400 PMMA SI-POF with 400 μm cladding diameter and $\text{NA} = 0.5$ was used. Four 60-cm-long fibers were terminated at the input side with 400 μm FC connectors. The opposite ends of the fibers were joined together and glued inside 970 μm FC connector to form the fiber bundle (**Figure 18**). As illustrated in **Figure 18**, an FC connector-mating sleeve was used to bring together and align the bundle and the input of the SI-POF link, thereby forming the multiplexing interface. An index-matching gel was applied between the connectors to reduce the losses.

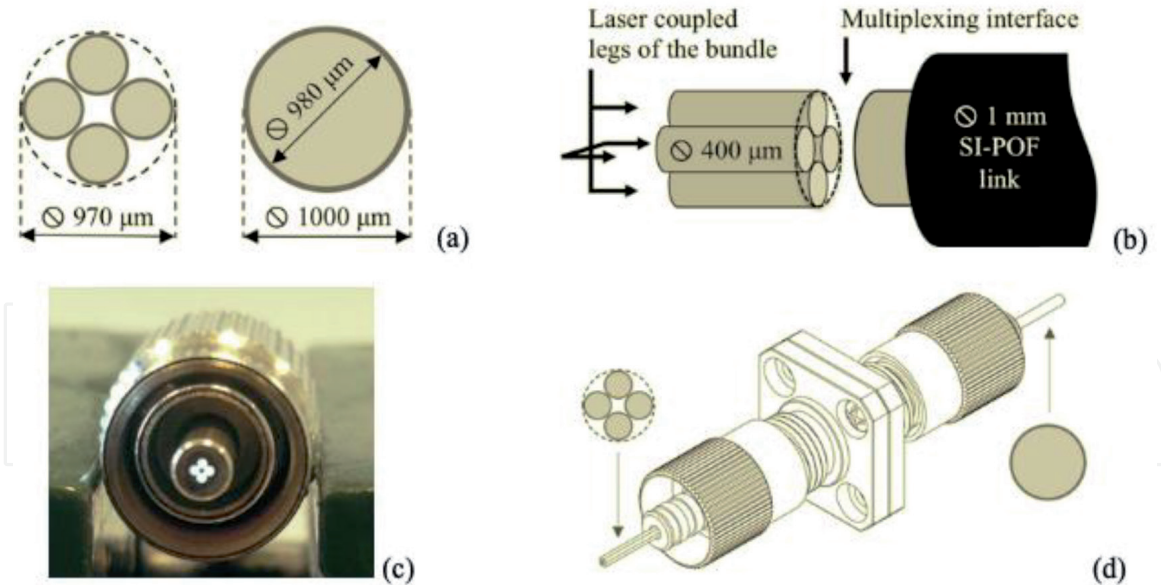


Figure 18.

Four-legged multiplexing POF bundle: (a) cross sections of four 400 μm cladding diameter fibers arranged within a circle with 970 μm diameter (left) and of 980/1000 μm SI-POF (right); (b) principle of operation of the POF bundle as a multiplexer; (c) four 400 μm fibers glued within 970 μm FC connector; (d) formation of a multiplexing interface with the POF bundle aligned against the SI-POF link using an FC connector-mating sleeve.

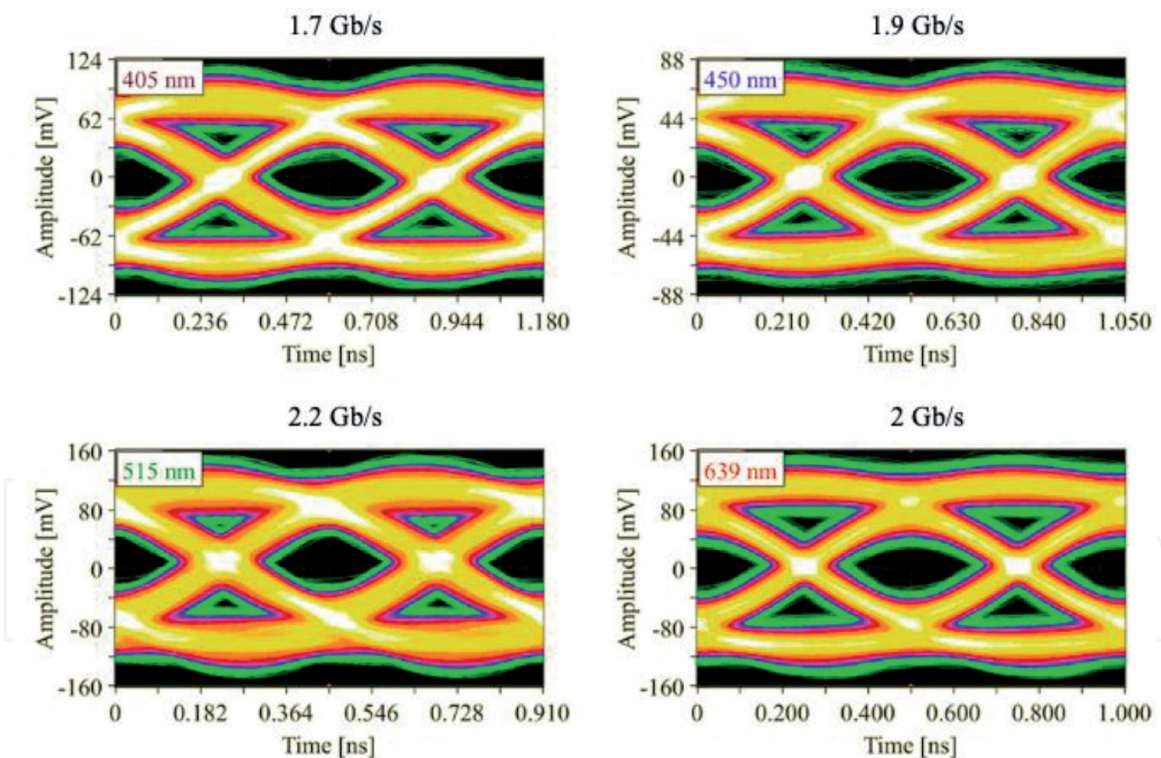


Figure 19.

Eye diagrams for 50 m SI-POF link at an aggregate bit rate of 7.8 Gb/s.

The described multiplexing solution was first shown in [29]. Shortly before, the patent application for an optical POF multiplexer based on a multi-legged POF bundle, which referred to arbitrary channel counts and fiber diameters, was submitted to the German Patent and Trade Mark Office (DPMA) under number DE 102013 020236.1. A similar approach was later adopted in [30, 31] to realize the low loss seven-legged and three-legged multiplexers, respectively.

The AWG simultaneously generated four independent NRZ data streams (Figures 16 and 19) based on 27-1 PRBS with the maximum sampling rate.

Operating wavelength [nm]	405	450	520	639
Laser diode-to-400 μm fiber launching loss + attenuation of a bundle leg [dB]	4.06	2.63	2.82	4.76
Connector loss (with index-matching gel) [dB]	0.87	0.98	0.52	0.77
Total loss [dB]	4.93	3.61	3.34	5.53

Table 7.

Optical power loss at the transmitter side when using four-legged POF bundle.

The received electrical signals were acquired by the real-time oscilloscope with 8-bit vertical resolution and oversampling. The digital receiver equalization was carried out in the offline mode. For that purpose the oscilloscope's built-in Serial Data Equalization software was used [32].

To prevent the equalizer from amplifying the noise components at higher frequencies where the energy content of useful signal was low, the bandwidth of the oscilloscope was set to the value in GHz corresponding to one half of the data rate in Gb/s. A phase-locked loop was used to extract the clock from the equalized data.

The eye diagram of an equalized waveform was displayed on the oscilloscope's screen for further analysis. The oscilloscope's built-in software EZJIT Complete was used to estimate the corresponding Q-factor [33]. Thereby, only a small time window (2% of the unit interval) in the middle of the equalized eye diagram was taken into consideration. The BER value was then calculated using Eq. (5). **Table 7** shows the optical power losses of the four used WDM channels.

6.5.7.8 Gb/s transmission over 50 m SI-POF

The WDM channels based on 405 nm (DL-7146-101S), 450, 515, and 639 nm laser diodes were employed in this transmission experiment. To maximize the modulating signal amplitude and thereby improve the SNR of the received signal, the optical output power of each laser diode was adjusted to its maximal possible value. For 405, 450, and 515 nm devices, the operating point was set to comply with the upper limit of the receiver's dynamic range. The 639 nm device was driven with the maximum recommended forward current. The respective used bias currents were 70, 40, 61, and 43 mA. The optical powers coupled into the SI-POF link and the received optical powers measured after the demultiplexer are given in **Table 7**. All diodes were driven in their linear lasing region. The 1 Vpp output amplitude of the AWG was sufficient to modulate 450, 515, and 639 nm laser diodes with the modulation index of approx. 0.9. The signal in 405 nm channel was additionally amplified to achieve the same modulation index. For the amplification, a MERA-556+ wideband amplifier (20.5 dB gain at 0.1 GHz) was used in combination with 10 dB attenuator to avoid amplifier nonlinearities (18 dBm output power at 1 dB compression point at 0.1 GHz).

The maximum transmission rates achieved in the individual channels were 1.7 Gb/s (405 nm channel), 1.9 Gb/s (450 nm channel), 2.2 Gb/s (515 nm channel), and 2 Gb/s (639 nm channel). Thereby, six FFE taps with the tap delay equal to one half of the corresponding bit period were used in each of the channels. The transmission parameters for the individual channels are listed in **Table 8**. The resulting eye diagrams are represented in **Figure 19**. A total of 7.8 Gb/s were transmitted over 50 m SI-POF at the $\text{BER} < 10^{-5}$. After deduction of 3.2% redundant bits required for Reed-Solomon (255,247) FEC, a net bit rate of 7.56 Gb/s was obtained. Compared to the record capacity of a single-channel system over the same fiber length used by Vinogradov et al. [10], an improvement of 1.67 Gb/s was achieved.

Operating wavelength [nm]	405	450	515	639
Bit rate [Gb/s]	1.7	1.9	2.2	2
Q-factor	5.06	4.67	4.96	4.76
BER	$2.10 \cdot 10^{-7}$	$1.51 \cdot 10^{-6}$	$3.52 \cdot 10^{-7}$	$9.68 \cdot 10^{-7}$

Table 8.
Transmission parameters for 50 m SI-POF link at an aggregate bit rate of 7.8 Gb/s.

7. Conclusions

We experimentally demonstrated the feasibility and potential of a high-speed POF WDM concept; a four-channel data transmission setup was realized. A four-legged multiplexing POF bundle was developed to combine the signals from four visible laser diodes onto SI-POF link. For the separation of wavelength channels, the interference filter-based demultiplexer with two-stage configuration was used. It was shown that POF WDM with lower channel rates and simple transmission technique (NRZ + FFE) could provide aggregate bit rates comparable to those achieved with the single-wavelength systems that used advanced modulation formats (DMT or PAM + DFE) and required significant signal processing. In addition, the 50 m SI-POF link at an aggregate bit rate of 7.8 Gb/s was demonstrated over 50 m SI-POF, respectively, at the BER = 10^{-3} .

Acknowledgements

We gratefully acknowledge the funding by the German Ministry of Education and Research (BMBF) under grant number 16V0009 (HS Harz)/16V0010 (TU BS). All injection molded parts are done with the support of the Institute of Micro and Sensor Systems at the Otto von Guericke University Magdeburg and Prof. Bertram Schmidt.

Author details

Ulrich H.P. Fischer-Hirchert* and Mladen Joncic
Harz University of Applied Sciences, Wernigerode, Germany

*Address all correspondence to: ufischerhirchert@hs-harz.de

IntechOpen

© 2019 The Author(s). Licensee IntechOpen. This chapter is distributed under the terms of the Creative Commons Attribution License (<http://creativecommons.org/licenses/by/3.0>), which permits unrestricted use, distribution, and reproduction in any medium, provided the original work is properly cited. 

References

- [1] Fischer-Hirchert UHP, Haupt M, Joncic M. Optical transmission systems using polymeric fibers. In: Predeep P, editor. *Optoelectronics—Devices and Applications*. Intech Open; 2011 Chapter 22
- [2] IEC09, Specification T. TS 105 175-1—V1.1.1—Access, Terminals, Transmission and Multiplexing (ATTM); Plastic Optical Fibre System Specifications for 100 Mbit/s and 1 Gbit/s. 2010. 1: pp. 1-16
- [3] Grzemba A. MOST. The Automotive Multimedia Network. From MOST25 to MOST150. Poing: Franzis; 2011. p. 250
- [4] Access, Terminals, Transmission and Multiplexing (ATTM); Plastic Optical Fibres; Part 1: Plastic Optical Fibre System Specifications for 100 Mbit/s and 1 Gbit/s; Sub-Part 2: 1 Gbit/s and 100 Mbit/s Physical Layer for Plastic Optical Fibres, ETSI Technical. 2015
- [5] Unified high-speed wireline-based home networking transceivers—System architecture and physical layer specification, ITU-T Recommendation G.9960. December 2011
- [6] Vinogradov J, Ziemann O, Lednicky O, Gottschalk J, Zceh M, Tchoupkoua S. Optimal equalizers for SI-POF and Gpbs. In: 17th Int Conf Plast Opt Fibers. 2008
- [7] Loquai S, Kruglov R, Schmauss B, Bunge C-A, Winkler F, Ziemann O, et al. Comparison of modulation schemes for 10.7 Gb/s transmission over large-core 1 mm PMMA polymer optical fiber. *IEEE Journal Light Technology*; **31**(13):2170-2176
- [8] Breyer F. Multilevel transmission and equalization for polymer optical fiber systems. Ph.D. dissertation, Germany: Fakultät für Elektrotechnik und Informationstechnik, Technische Universität München; 2010
- [9] Lee SCJ. Discrete multitone modulation for short-range optical communication. Ph.D. dissertation, Netherlands: Department of Electrical Engineering, Eindhoven University of Technology; 2009
- [10] Vinogradov J, Kruglov R, Loquai S, Ziemann O. Multi gigabit transmission with blue, green and red laser diodes. In: 20th International Conference on Plastic Optical Fibers; 2011. pp. 467-470
- [11] Joncic M, Haupt M, Fischer UHP. Investigation on spectral grids for VIS WDM applications over SI- POF Untersuchung von Spektralen Gittern für VIS WDM-Anwendungen über SI-POF. In: ITG Fachtagung Photonische Netze. Leipzig: VDE Verlag; 2014. p. 38855
- [12] Lekishvili N, Nadareishvili L, Zaikov G, Khananshvili L. *Polymers and Polymeric Materials for Fiber and Gradient Optics*. Amsterdam: Brill Academic Publishers; 2002
- [13] Bunge C-A. Private communication—spectral attenuation of Asahi fiber specified for MOST
- [14] Koike Y. *Fundamentals of Plastic Optical Fibers*. Hoboken, New Jersey: Wiley and Sons, Inc.; 2014
- [15] Kaino T. In: Jones W, editor. *Organic Molecular Solids: Properties and Applications*. London: CRC Press; 1997. p. 352
- [16] Emslie C. Review polymer optical fibers. *Journal of Materials Science*. 1988;**23**:2281-2293
- [17] Groh W. Overtone absorption in macromolecules for polymer optical fibers. *Die Makromol Chemie*. 1988;**189**(12):2861-2874

- [18] Ziemann O, Krauser J, Peter EZ, Daum W. POF Handbook—Optical Short Range Transmission Systems. Berlin Heidelberg: Springer Verlag; 2008. p. 455
- [19] Thiele H-J, Nebeling M. Coarse Wavelength Division Multiplexing: Technologies and Applications. London: CRC Press, Taylor and Francis Group; 2007
- [20] LIGHTTEL Product specification. 4, 8, and 16 Channel Extended Band CWDM Mux/Demux. 2014
- [21] Dutta AK, Dutta NK, Fujiwara M. WDM Technologies: Passive Optical Components. Cambridge: Academic Press; 2003
- [22] Herbert V. Wavelength Filters in Fibre Optics. Berlin, Heidelberg: Springer; 2006
- [23] S. Proakis. Digital Communications. 5th ed., McGraw-Hill; 2008.
- [24] Lee SCJ, Breyer F, Randel S, Gaudino R, Bosco G, Bluschke A, et al. Discrete multitone modulation for maximizing transmission rate in step-index plastic optical fibers. *IEEE Journal Light Technology*. 2009;27(11):1503-1513
- [25] Loquai S, Kruglov R, Ziemann O, Vinogradov J, Bunge C.-A. 10 Gbit/s over 25 m plastic optical fiber as a way for extremely low-cost optical interconnection. In: OFC/NFOEC. 2010. paper OWA6
- [26] Joncic M, Höll S, Haupt M, Caspary R, Fischer UHP. Development status of a four-channel CWDM system for multi-Gbit/s data links over SI-POF. In: 22nd International Conference on Plastic Optical Fibers; 2013. pp. 59-64
- [27] Diaz E, Knobl M. Prototyping illumination systems with stock optical components. *Photonik International*. 2012;2:4-7
- [28] Appelt V, Vinogradov J, Ziemann O. Simple FEXT compensation in LED based POF-WDM systems. In: 11th International Conference on Plastic Optical Fibers; 2002. pp. 127-129
- [29] Jončić M, Haupt M, Fischer UHP. Development status of a four-channel CWDM system for Multi-Gbit/s in-house data communication via SI-POF. In: 20 ITG-Fachtagung Kommun. 2013; pp. 6
- [30] Kruglov R, Vinogradov J, Loquai S, Ziemann O, Bunge C-A, Hager T, Strauss U. 21.4 Gb/s discrete multitone transmission over 50-m SI-POF employing 6-channel WDM. In: OFC/NFOEC; 2014. p. Paper Th2A.2
- [31] Pinzon PJ, Vasquez C, Perez I, Lallana PC. Design and analysis of a WDM system for multi-Gbit/s transmission over 50 m of SI-POF. In: 23rd International Conference on Plastic Optical Fibers; 2014
- [32] Agilent Technologies I. User's guide. Agilent N5461A Infiniium Serial Data Equalization [Online]. 2009
- [33] Agilent Technologies I. Data sheet. EZJIT Complete Jitter and Vertical Noise Analysis Software for Infiniium Oscilloscopes [Online]. 2013